Journal of Engg. Research Vol.10 No. (1A) pp. 330-346 DOI: 10.36909/jer.13185

Predicting the Flow Zone Indicator of Carbonate Reservoirs using NMR Echo Transforms and Routine Open-Hole Log Measurements: Insights from a Field Case Study Spanning Extreme Microstructure Properties

Mabkhout Al-Dousari*, Salah Almudhhi and Ali A. Garrouch

** Petroleum Engineering Department, Kuwait University*
** Corresponding Author: dr.aldousari@ku.edu.kw*

Submitted *:* 07/02/2021
Revised *:* 21/07/2021
Accepted *:* 04/08/2021

ABSTRACT

Predicting the flow zone indicator is essential for identifying the hydraulic flow units of hydrocarbon reservoirs. Delineation of hydraulic flow units is crucial for mapping petrophysical and rock mechanical properties. Precise prediction of the flow zone indicator (FZI) of carbonate rocks using well log measurements in un-cored intervals is still a daunting challenge for petrophysicists. This study presents a data mining methodology for predicting the rock FZI using NMR echo transforms, and conventional open-hole log measurements. The methodology is applied on a carbonate reservoir with extreme microstructure properties, from an oil "M" field characterized by a relatively high-permeability with a median of approximately 167 mD, and a maximum of 3480 mD. The reservoir from the M field features detritic, or vuggy structure, covering a wide range of rock fabrics varying from microcrystalline mudstones to coarse-grained grainstones. Porosity has a median of approximately 22%. Dimensional analysis and regression analysis are applied for the derivation of four transforms that appear to capture approximately 80% of the FZI variance. These four transforms are formulated using the geometric mean of the transverse NMR relaxation time (T_{2lm}), the ratio of the free fluid index (FFI) to the bulk volume irreducible (BVI), the bulk density, the sonic compressional travel time, the true resistivity, the photo-electric absorption, and the effective porosity. Non-linear regression models have been developed for predicting the FZI using the derived transforms, for the carbonate reservoir from the M field. The average relative error for the estimated FZI values is approximately 52%. The same transforms are used as input for training a developed general regression neural network (GRNN), built for the purpose of predicting rock FZI. The constructed GRNN predicts FZI with a notable precision. The average absolute relative error on FZI for the training set is approximately 3.1%. The average absolute relative error on FZI for the blind testing set is approximately 22.0 %. The data mining approach presented in this study appears to suggest that (i) the relationship between the flow zone indicator and open-hole log attributes is highly non-linear, (ii) the FZI is highly affected by parameters that reflect rock texture, rock

microstructure geometry, and diagenetic alterations, and (iii) the derived transforms provide a means for further enhancement of the flow zone indicator prediction in carbonate reservoirs.

Keywords: Flow zone indicator; Carbonate rocks; Dimensional analysis; Open-hole log data; Rock typing; NMR T_2; Neural networks.

Nomenclature

a = 49.395 b = 1.0148 c = 0.13

F	resistivity formation factor
k	permeability (mD)
L	basic dimension of length
M	basic dimension of mass
P_e	photo-electric absorption (barns/electron)
Q	fundamental dimension of charge
R_t	true resistivity (Ωm)
R_w	resistivity of reservoir water at T_F (Ωm)
R_{wa}	apparent resistivity of formation water (Ωm)
T	basic dimension of time

Acronyms

BVI	bulk volume irreducible
DRT	discrete rock type
DT	acoustic compressional wave travel time
FZI	flow zone indicator
FFI	free fluid index
GR	gamma ray log response

Symbols

λ_o = 19.546 λ_1 = 2.8788 λ_2 = -9.3494

λ_3 = -10.25 λ_4 = -1.5955 λ_5 = -6.6707 λ_6 = 6.7833

ϕ_z	normalized porosity index
ϕ_e	effective porosity
λ_r	dimensionless FZI
λ_z	dimensionless Permeability number
Ω_1	dimensionless resistivity number
Ω_2	dimensionless pore radius transform
Δt	travel time of the compressional acoustic wave (μsec/ft)
ρ_b	response of the density log (gm/cm^3)
τ	coefficient

INTRODUCTION

In recent years, rock typing has been accepted as an essential key tool for reservoir characterization. Without a robust mapping of rock types across the reservoir, prediction of the reservoir static and dynamic petrophysical rock properties becomes a perplexing task (Corbett and Mousa, 2010; Parsad, 2003; Panjamani et al., 2016). Indeed,

rock typing is fundamental in a number of applications like static and dynamic reservoir modeling, preparing production management plans for oil and gas fields, and predicting reservoir rock mechanical properties. The latter properties are crucial for hydraulic fracturing design, sand production management, and for horizontal and multi-lateral well placement. Recently, it has become increasingly evident that mapping of petrophysical and rock mechanical properties are reliable only when based on rock type segregation (Michel and Bruno, 2014). A rock type is a geologically and petrophysically distinct and homogeneous rock interval featuring unique relationships between petrophysical properties. A rock type possesses a well-defined link with lithology, deposition environment, and diagenesis. Rock intervals with resembling geological facies and texture properties generally are of the same rock type, and therefore, have common petrophysical properties (Prasad, 2003).

Michel and Bruno (2014) give a thorough review of various rock typing methods available in the literature. Ideally, rock types account for two fundamental controls which consist of (i) the depositional texture control which describes the size and shape of the grains, the grain packing, grain orientation, facies fabric, and sorting characteristics and (ii) the diagenesis control which includes dissolution, cementation, dolomitization, fracturing, recrystallization, and compaction (Sneider and Erickson, 1997; Riazi, 2018; Mirzaei-Paiaman et al., 2018; Soleymanzadeh et al., 2018). Amaefule et al. (1993) and Guo et al. (2007) are among the researchers who made use of the flow zone indicator (FZI) to delineate various rock types. A discrete rock type (DRT) is defined using the flow zone indicator (FZI), as follows (Guo et al. 2007; Ghadami et al., 2015):

$$DRT = Round\left[2\ln\left(FZI\right)+10.6\right]. \tag{1}$$

The DRT appears to delineate hydraulic flow units featuring similar pore topology, and geological framework having similar petrophysical properties (Michel and Bruno, 2014). Rock intervals of equal DRT values, presumably, fit in the same hydraulic flow unit (Guo et al., 2007; Gunter et al., 1997; Abedini et al., 2011). The rock typing methodology proposed in this study is founded on the measurements of porosity and permeability. This methodology circumvents the awkward rock typing techniques that relies on mercury injection capillary pressure (MICP) data, as well as thin section observations which are occasionally unavailable (Michel and Bruno, 2014). Moreover, MICP derived pore size distributions are plagued by a major inconsistency since they account for only the pore volume accessible through the pore throats, at an applied fixed pressure. If for instance, large pore bodies are accessible only through small pore throats, the large pore body structure might not be reflected in the final pore size distribution.

Amaefule et al. (1993) relate the flow zone indicator to rock texture properties as follows:

$$FZI = \frac{1}{\sqrt{F_s \tau S_{vgr}}}. \tag{2}$$

In the above notation, τ is rock tortuosity, S_{vgr} is the specific surface area per unit grain volume, and F_s is the pore shape factor. The latter parameter generalizes the capillary-tube model derived by Kozeny-Carman to a porous medium having a distribution of pore shapes (Prasad, 2003), as follows:

$$k = \frac{1}{F_s \tau^2 S_{vgr}^2} \frac{\phi_e^3}{\left(1-\phi_e\right)^2}. \tag{3}$$

For a bundle of capillary tubes of circular cross section, parameter F_s assumes a value of 2 (Prasad, 2003). By combining Equations (2) and (3), the FZI can be estimated using laboratory measurements of permeability and effective porosity as follows:

$$FZI = \frac{0.0314\left(1-\phi_e\right)}{\phi_e}\sqrt{\frac{k}{\phi_e}}. \tag{4}$$

In the above notation, k is the absolute permeability in mD, FZI is given in μm, and ϕ_e is the effective porosity input as a fraction.

As suggested by Prasad (2003), the FZI appears to reflect connectivity between pores. In simple terms, larger FZI values imply a high level of connectivity between pores, and hence higher permeability values. This is the case for fractured rocks, and for highly sorted rocks with large grains and with little clay content. Growth of authigenic clays, compaction, lack of sorting, diagenetic alteration of constituent minerals, and cementation of grains act to decrease connectivity. A decrease in connectivity causes a decrease in FZI and, consequently, permeability.

Delineation of carbonate rock types using well log data is generally a complex task, and results are usually fraught by significant uncertainty. This is partially due to the high level of heterogeneity associated with carbonate rocks. Indeed, heterogeneity of carbonate rocks emanates from the complex micro-structure geometry of the pore network. The solid framework of carbonate rocks is composed mainly of particles having biological and non-biological origin embedded in partially lime-mud matrix, or in a cementing material. The size and shape distribution of these particles augmented with micro-fractures, and with the intense diagenesis over time, cause the high level of heterogeneity in these rocks.

The objective of this research is to gain insights into variables and transforms that impact the rock flow zone indicator. The ability of the NMR log-derived transverse relaxation time (T_2) distribution to reflect vividly the microstructure geometry of rocks positions the NMR echo transforms as key information tools that may help alleviate the difficulty encountered in carbonate rock typing (Coates et al., 1999). Parameter T_2, which replicates the magnetization rate loss of hydrogen protons in pores, is given as a function of the pore surface to volume ratio (S/V) as follows (Coates et al., 1999):

$$\frac{1}{T_2} = \frac{1}{T_{2bulk}} + \rho_2\frac{S}{V} + \frac{D\left(\gamma GTE\right)^2}{12}. \tag{5}$$

In the above notation,

ρ_2	is the surface relaxivity.
T_{2bulk}	is the bulk fluid transverse relaxation time.
D	is fluid diffusion coefficient.
γ	is the gyromagnetic ratio of a hydrogen proton
G	is magnetic field-strength gradient.
TE	is the echo spacing, or time between 180^o pulses.

The dependence of T_2 on the pore surface to volume ratio (S/V) makes it profoundly sensitive to rock texture. This fact implicates T_2 and its attributes as potentially prominent variables for modeling rock FZI.

The next section illustrates how the proposed data mining methodology is applied for predicting rock FZI using M field data described in Appendix A.

FORMULATION OF PETROPHYSICAL TRANSFORMS

Formulation of a Dimensionless Resistivity Transform (Ω_1)

The first transform is formulated by intuitively postulating a generic relationship for the FZI as a function of the wireline log responses (Garrouch and Al-Sultan, 2019), as follows:

$$FZI = f(\Delta t, \rho_b, P_e, R_t, R_{wa}). \tag{6}$$

In the above notation,

R_{wa} is the apparent water resistivity (ohm-m).
P_e is the photo-electric absorption (barns/electron).
ρ_b is the bulk density (gm/cm^3).
Δt is the compressional sonic wave travel time (μsec/ft).
R_t is the true resistivity (ohm-m).

An *MLTQ* dimensional analysis, for the dependence of the flow zone indicator on conventional well log readings, was performed in order to formulate crucial dimensionless groups. The terms *M, L, T, and Q* represent the fundamental dimensions of mass (*M*), length (*L*), time (*T*), and charge (*Q*). Table 1 lists the basic dimensions and units of all variables used in the dimensional analysis. Given the six variables expressed in Equation (6), and the four basic dimensions (*MLTQ*), Buckingham's pi theorem allocates two dimensionless numbers (λ_1 and Ω_1), given as follows (Garrouch and Al-Sultan, 2019):

$$\lambda_1 = \frac{FZI \cdot P_e^2}{\Delta t \cdot \rho_b \cdot R_{wa}}, \tag{7}$$

$$\Omega_1 = R_t \left(\frac{\Delta t^2 R_{wa}}{\rho_b{}^2 P_e^8} \right)^{1/3}, \tag{8}$$

Table 1. Basic dimensions of dependent and independent variables.

Variable	Symbol	Unit	Dimension
Interval transit time	Δt	μsec/ft	$L^{-1}T$
Bulk density	ρ_b	gm/cm^3	$M L^{-3}$
Photo-electric absorption	P_e	barn/e	L^2Q^{-1}
True resistivity	R_t	Ωm	$ML^3T^{-}Q^{-2}$
Permeability	k	mD	L^2
Characteristic pore radius	r_p	μm	L
Flow zone indicator	*FZI*	μm	L

Group λ_1 given by Equation (7) is denoted as dimensionless FZI. Group Ω_1 given by Equation (8) is denoted as dimensionless resistivity. The transform Ω_1 will be used later for modeling the FZI.

Formulation of a Dimensionless Pore Radius Transform (Ω_2)

Dimensional analysis is applied henceforth to formulate dimensionless transforms that link rock permeability (k) to open-hole log measurements. These transforms are formulated by intuitively postulating a generic relationship for the permeability as a function of open-hole log measurements and attributes, given by the following equation:

$$k = f(\Delta t, \rho_b, P_e, R_t, r_p). \tag{9}$$

In the above equation, r_p is a characteristic pore radius estimated using the geometric average of the NMR transverse relaxation time distribution (T_{2lm}) and the surface relaxivity (ρ_2), as follows (Coates et al., 1999):

$$r_p = \frac{2T_{2lm}\rho_2}{1000} \quad . \tag{10}$$

In the above notation, ρ_2 is the surface relaxivity in μm/sec and r_p is in μm. T_{2lm} is in msec. In this analysis, *k* and r_p stand for the non-repeating variables. The parameters Δt, ρ_b, P_e, and R_t stand for the repeating variables. The following two dimensionless groups are formulated, as a consequence:

$$\lambda_2 = \frac{k\rho_b^2 P_e^4}{\Delta t^2 R_t^2}, \tag{11}$$

$$\Omega_2 = \frac{r_p \rho_b}{\Delta t P_e^2 R_t}. \tag{12}$$

The dimensionless group (λ_2) is denoted as a dimensionless permeability transform. The dimensionless group (Ω_2) is denoted as a dimensionless pore radius transform which is the main outcome of this analysis. The transform Ω_2 will be used later for modeling the FZI.

Formulation of an FZI Transform (T_r)

A reverse engineering approach has been implemented for deriving a transform that captures a significant proportion of the FZI variance. The procedure consists of constructing a rock texture parameter ( ) that may be regarded as a weighted geometric mean of two characteristic pore radii: one obtained from the NMR transverse relaxation time distribution (Equation (10)) and the other obtained from routine core measurements of permeability and porosity, expressed as follows (Garrouch, 1999):

$$\overline{r}_p = \frac{2\sqrt{2}\tau}{\sqrt{1000}}\sqrt{\frac{k}{\phi_e}}. \tag{13}$$

The rock texture parameter (Ψ) is expressed as a function of the geometric mean of the NMR transverse relaxation time distribution (T_{2lm}), permeability (k), effective porosity (ϕ_e), and tortuosity (τ) as follows:

$$\Psi = \left[\left(T_{2lm}^{7} 2\sqrt{2}\tau\sqrt{\frac{k}{1000\phi_e}}\right)\right]^{c}. \tag{14}$$

In the above notation, c is a constant given in the nomenclature. The rock tortuosity is approximated as follows (Garrouch, 1999):

$$\tau = \frac{1}{\phi_e}. \tag{15}$$

The rock texture parameter Ψ is plotted versus the derived characteristic pore radius (r_p) obtained using Equation (10), using the carbonate reservoir data from the M field. Figure 1 depicts a power-law relationship between variable Ψ and r_p, with a determination coefficient of approximately 0.99. This power-law relationship may be expressed as follows:

$$\Psi = a\, r_p^{b} \tag{16}$$

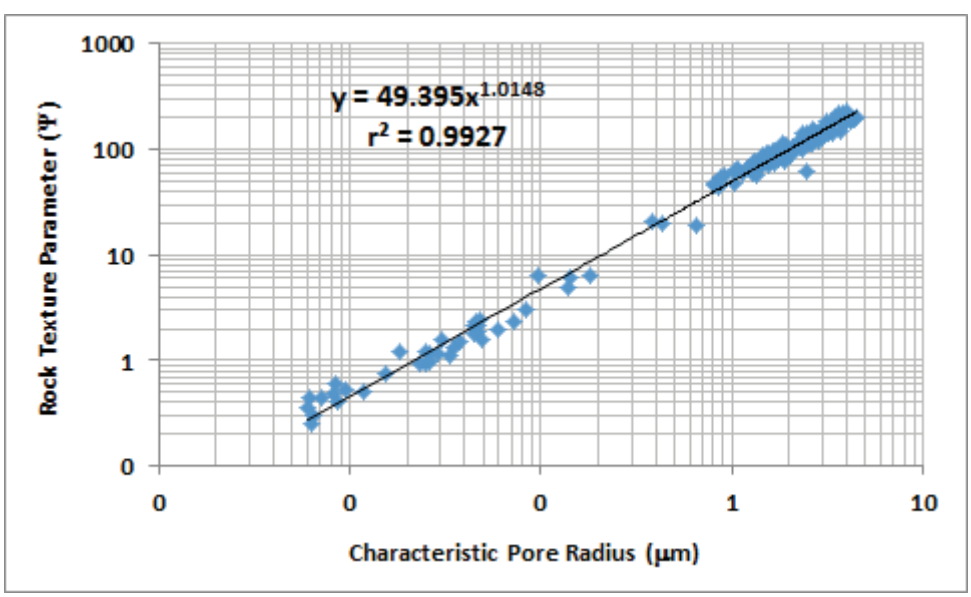

Figure 1. Rock texture parameter (Ψ) versus characteristic pore radius (r_p), for the carbonate reservoir from the M field.

Equation (16) is rearranged by substituting the expression of Ψ from equation (14) and the expression of tortuosity from equation (15) as follows:

$$\sqrt{\frac{k}{\phi_e}} = \left[\frac{\phi_e\sqrt{1000}}{2\sqrt{2}T_{2lm}^7}\right]\left(a\,r_p^b\right)^{1/c}. \tag{17}$$

A flow zone indicator transform (T_r), equivalent to the FZI expression given by equation (4), is derived from Equation (17) as follows:

$$T_r = \left[\frac{0.351\left(1-\phi_e\right)}{T_{2lm}^7}\right]\left[ar_p^b\right]^{1/c}. \tag{18}$$

The above transform does not include permeability. Parameter r_p is estimated using Equation (10) from NMR T_{2lm} data. Therefore, if the transform of Equation (18) captures a significant amount of the FZI variance, it might be an important parameter for modeling the FZI. A confirmation would be obtained by plotting the derived transform as a function of the FZI. Figure 2 displays a plot of the transform T_r versus FZI, for the carbonate reservoir from the M field. The relationship is indeed fraught by some scatter, characterized by an overall positive correlation. The power-law relationship between T_r and FZI appears to have a coefficient of determination of approximately 0.67. This is a comforting fact since it implies that transform T_r alone is capable of capturing about 67% of the FZI variance.

The next section integrates the developed transforms (Ω_1, Ω_2, T_r) with NMR log attributes to come up with a non-linear regression model for predicting the FZI.

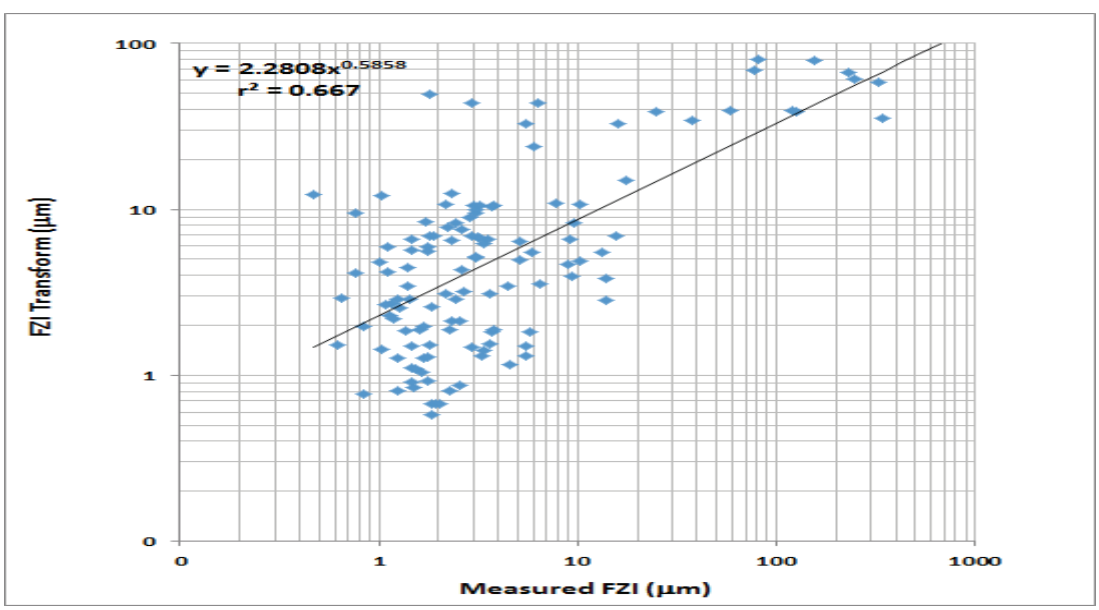

Figure 2. FZI transform versus measured FZI for the carbonate reservoir from the M field.

REGRESSION MODELING THE FLOW ZONE INDICATOR

Intuitively, any mathematical expression of FZI has to depend on variables that reflect rock texture (Lucia, 2007). The previously introduced transforms (Ω_1, Ω_2, T_r) and the effective porosity (ϕ_e) are among these variables. Additional texture dependent parameters are obtained from the NMR attributes like FFI and BVI. A generic expression between FZI and texture dependent variables may, therefore, be generalized as follows:

$$FZI = f\left(T_r, \Omega_1, \Omega_2, \left(\frac{FFI}{BVI}\right)^2, \phi_e\right). \tag{19}$$

A linear regression model between FZI and the remaining variables of Equation (19) gives a determination coefficient equal to 0.42. As evidenced by the values of the coefficients of skewness (Table 2), FZI of the carbonate reservoir from the M field, parameters ϕ_e, r_p, and T_{2lm}, FFI, and the BVI appear to have a coefficient of skewness different from zero. Thus, these variables may be represented by log-normal distributions. As a consequence, another generic implicit expression for FZI is proposed as follows:

$$\log\left(FZI\right) = f\left(\log\left(T_r\right), \log\left(\Omega_1\right), \log\left(\Omega_2\right), \log\left(\frac{FFI}{BVI}\right)^2, \log\left(\phi_e\right)\right). \tag{20}$$

A regression model between log (FZI) and the variables to the right-hand-side (RHS) of Equation (20), for the carbonate reservoir from the M field, gives the following empirical model:

$$\begin{aligned}\log FZI = a_0 + a_1 log T_r + a_2 log\Omega_1 + a_3 log\Omega_2 + a_4 \log\left(FFI / BVI\right)^2 + \\ + a_5 log\phi_e + a_6 log T_{2lm}\end{aligned} \tag{21}$$

The regression coefficients a_0, a_1, a_2, a_3, a_4, a_5, and a_6, are given in Table 3. The determination coefficient of M field reservoir measurements equals 0.81. Figure 3 displays a plot of estimated FZI versus core-measured FZI values for the carbonate reservoir from the M field. The FZI values were estimated using the regression model given by Equation (21). The average absolute relative error on FZI obtained using the model given by equation (21) is approximately 65%.

Table 2. Summary statistics of the carbonate reservoir from the M field.

Variable	Minimum	Maximum	Median	Mean	Standard deviation	Skewness
FZI (m)	*0.58*	379.12	5.64	30.77	62.12	2.99
R_{wa} (ohm-m)	*0.0005*	7.791	0.091	0.892	1.418	2.119
R_t (ohm-m)	*0.51*	1950	14.4	40.4	168.1	10.8
b (gm/cm3)	*2.16*	2.93	2.33	2.41	0.20	0.84

Pe (barn/e)	*3.63*	9.96	5.01	5.62	1.38	1.95
t (sec/ft)	*47.70*	91.63	76.42	73.27	12.19	-0.5
k (mD)	*11.0*	3480	167.2	458.3	669.2	2.28
Core	*0.9*	30.4	21.6	18.0	10.0	-0.71
T_{2lm} (msec)	*1.01*	748.34	280.3	281.37	214.22	0.22
FFI	*0.000*	0.263	0.194	0.152	0.098	-0.715
BVI	*0.000*	0.211	0.037	0.039	0.024	2.57
MPHI	*0.00*	31.97	23.47	19.05	10.78	-0.74
r_p (m)	*0.0061*	4.49	1.68	1.69	1.29	0.22

Table 3. Regression statistics the M field data.

Coefficient/field	Model given by Equation (21)	Model given by Equation (22)
a_0	11.78808	3.01422
a_1	3.56129	-1.55547
a_2	-0.05618	-0.421952
a_3	-0.10178	-3.05071
a_4	-0.01627	-0.0455548
a_5	4.890191	0.0
a_6	-2.71828	0.0
R^2	0.81	0.83
Number of observations	140	140

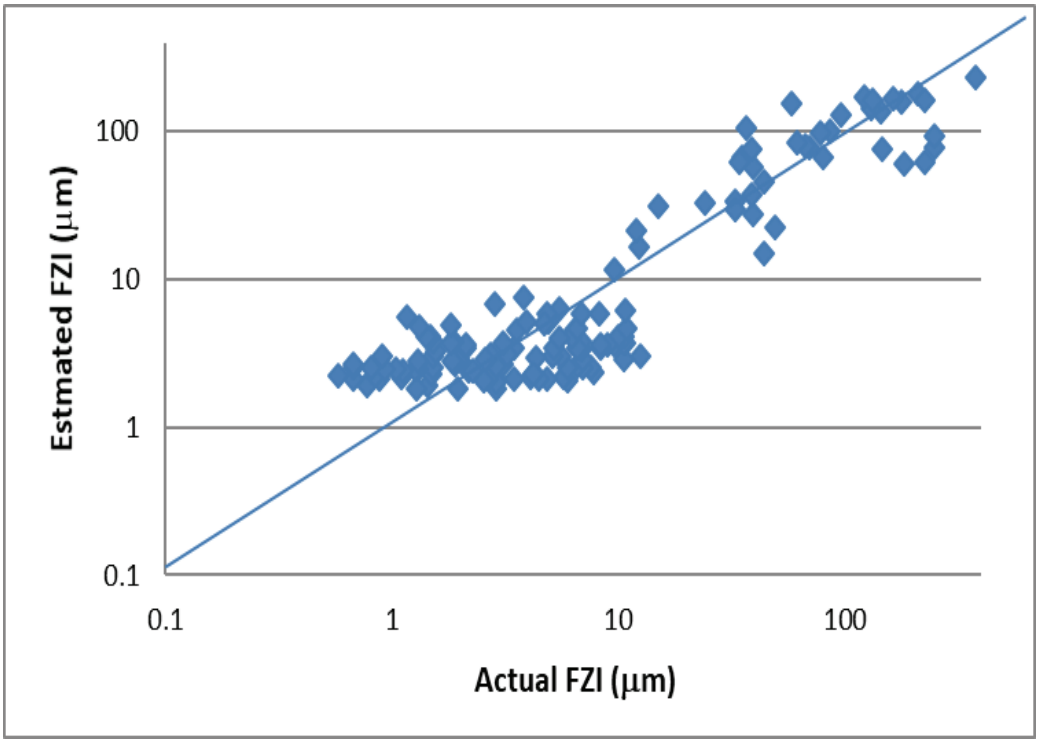

Figure 3. Estimated FZI versus measured FZI for the carbonate reservoir of the M field, using Equation (21).

A non-linear curve fitting software (ndCurveMaster) has been also used to find the best relationship between the variables given in Equation (20). An automated heuristic technique for data fitting is applied by use of a random iterated search algorithm in an ample search of approximately 360 basic power, exponential, and logarithmic functions. Final relationship between dependent and independent variables with the least amount of error between actual and predicted target variables is reported. The algorithm stops its search when the coefficient of determination value reaches its maximum. The following implicit relationship for FZI is obtained with a determination coefficient equal to 0.83:

$$\log\left(\mathrm{FZI}\right) = a_0 + a_1 e^{(\log(T_r))^{-0.5}} + a_2 e^{(\log(\Omega_1))^{0.5}} + a_3 e^{(\log(\Omega_2))^{0.5}} + a_4 e^{\log(\frac{\mathrm{FFI}}{\mathrm{BVI}})^2}. \quad (22)$$

The coefficients a_0, a_1, a_2, a_3, and a_4 of Equation (22) are given in Table 3. Figure 4 shows a comparison between the estimated FZI values using Equation (22), and measured FZI values. The average absolute relative error on FZI using Equation (22) is approximately 52%. This is an improvement of approximately 13% reduction in the relative error obtained using Equation (21). Nevertheless, Equations (21) and (22) affirm a highly non-linear relationship between FZI, the derived transforms, and the NMR log attributes. This is contrary to the linear relationship reported by Guo et al. (2007) between FZI and normalized conventional log responses, given as follows:

$$FZI = \lambda_0 + \lambda_1 NXRD + \lambda_2 NXRHO + \lambda_3 NXGR + \lambda_4 NXSP + \lambda_5 NXDT + \lambda_6 NXNPHI \quad (23)$$

In the above notation,

NXRD is dimensionless deep resistivity.
NXRHO *is* dimensionless bulk density measurement.
NXGR is dimensionless gamma ray measurement.
NXSP is dimensionless spontaneous potential measurement.
NXDT is dimensionless sonic travel time.
NXNPH is normalized neutron porosity measurement.

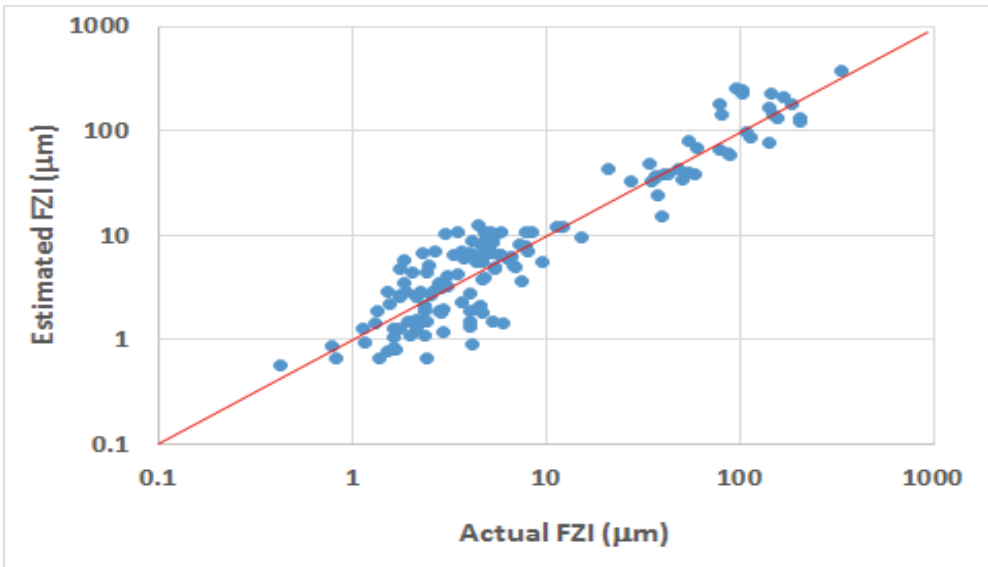

Figure 4. Estimated FZI versus measured FZI for the carbonate reservoir of the M field, using Equation (22).

The constants λ_0, λ_1, λ_2, λ_3, λ_4, λ_5, and λ_6 are given in the nomenclature. The dimensionless numbers of Equation (23) values are estimated using the following general expression:

$$N\chi = \frac{\chi - \chi_{\min}}{\chi_{\max} - \chi_{\min}}, \tag{24}$$

where

χ is a log measurement at an arbitrary depth,
$\chi_{\min}$ is the minimum measurement value of χ, and
$\chi_{\max}$ is the maximum measurement value of χ.

Figure 5 compares the estimated FZI values, using Guo et al. (2007) model, with measured FZI values. Guo et al. model (2007) was not able to match the actual FZI span, giving FZI estimates within two orders of magnitude variation of the measured FZI values. The average absolute relative error on FZI using Guo et al. (2007) model was approximately 520%.

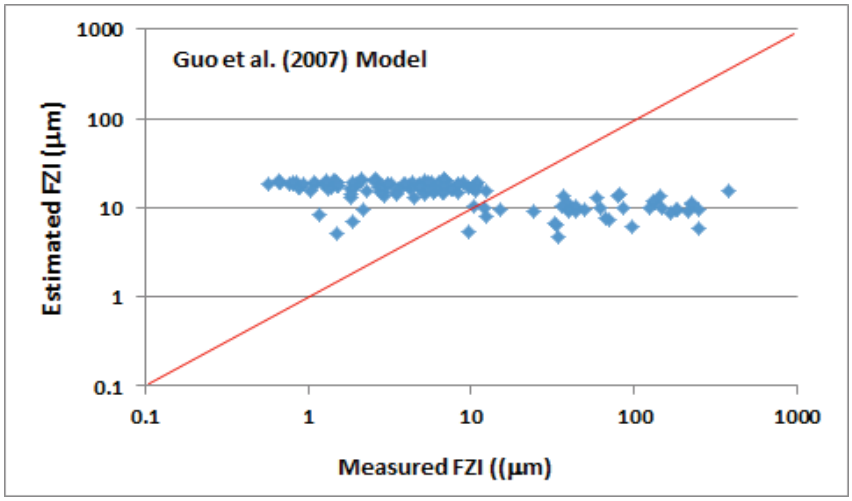

Figure 5. FZI estimated using Guo et al. model (2007) versus measured FZI for the carbonate reservoir of the M field.

NEURAL NETWORK MODELING OF THE FLOW ZONE INDICATOR.

Neural Network Paradigm.

Since the data used for developing the FZI model are relatively small (140 cored depths), a general regression neural network (*GRNN*) is constructed for the purpose of modeling the FZI as a function of the variables, expressed in Equation (20). The *GRNN* is suitable for performing non-linear regression for continuous target variables. This type of network has been used in the past for building models when variables are related by complex non-linear relationships (Al-Dousari et al., 2016). A GRNN features a connectionist parallel structure where learning does not involve any iteration. *GRNN* establishes an empirical joint distribution function using the available non-parametric estimators (Specht, 1991). *X* in this research analysis stands for the set of input parameters $\log(T_r)$, $\log(\Omega_1)$, $\log(\Omega_2)$, log(FFI/BVI), log(T2lm), and $\log(\phi_e)$. The target output variable *Y* stands for the log(FZI). The joint probability density function (pdf) and the algorithm for evaluating the conditional mean of the target output variable have been detailed by Al-Dousari et al. (2016). The *GRNN* algorithm has been realized in a GRNN structure shown in Figure 6. The GRNN structure consists of an input layer, a hidden layer, a summation layer, and an output layer.

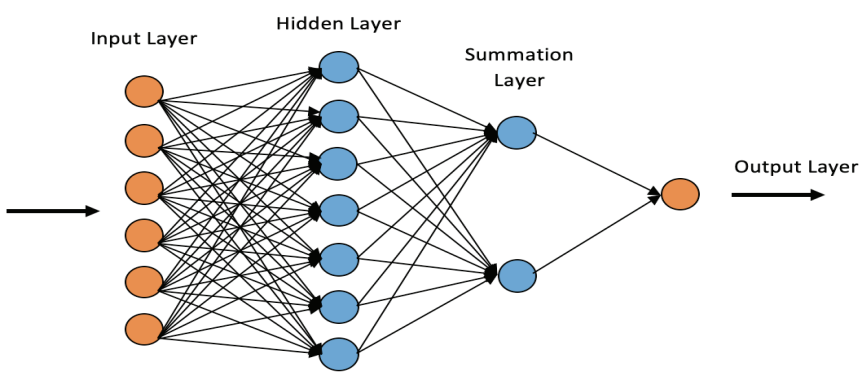

Figure 6. A schematic of the GRNN architecture used.

Training and Testing of the GRNN Paradigm

A total of 140 vectors, for the carbonate reservoir of the M field, with six input variables and one output variable, have been uploaded into NeuroShell software input file (Al-Dousari et al., 2016). NeuroShell divides the input file into a training data set composed of 90% of the data, and a blind-test data-set composed of the remaining 10% of the data. Figure 7 displays the network FZI versus the actual FZI for the training data set. A coefficient of determination of 0.99 is obtained. The average absolute relative error on FZI for the training set is approximately 3.1%.

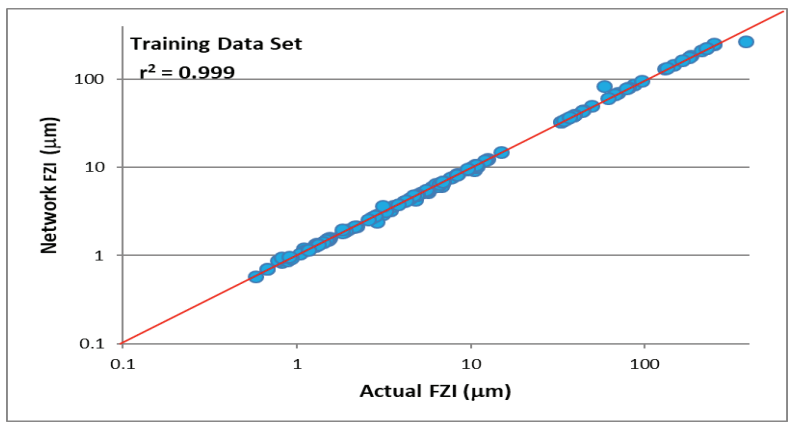

Figure 7 . FZI estimated from GRNN compared to measured actual FZI values for the training data set. Data belong to the carbonate reservoir from the M field.

This indicates that the network has established a relationship between the input and output variables. However, to make sure that network memorizing is not taking place, a test with a blind data set has to be performed. Figure 8 displays the network FZI versus the actual FZI for the blind testing data set. A coefficient of determination of approximately 0.97 is obtained for the blind test data set. The average absolute relative error on FZI for the blind testing set is approximately 22.0 %. It appears that the GRNN is able to generalize the model developed to a data set not seen by the network during training.

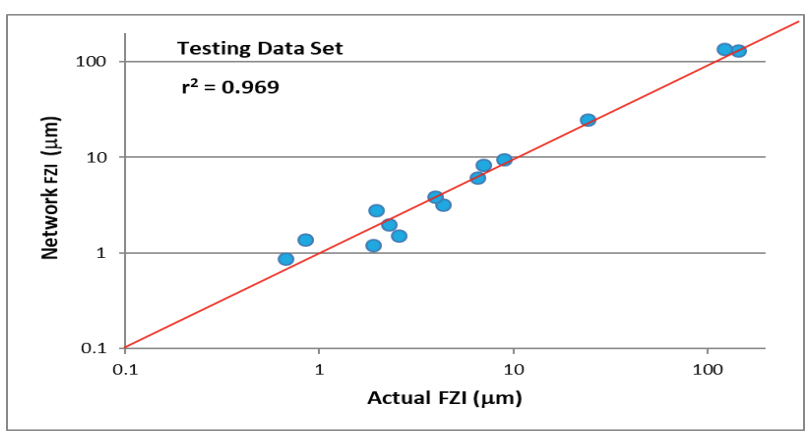

Figure 8. FZI estimated from GRNN compared to measured actual FZI values for the testing data set. Data belong to well the carbonate reservoir from the M field.

The precision of the *GRNN* model estimates, using the test data set, appears to be remarkable. It is concluded that the network is able to develop a non-linear model relating the logarithm of FZI to open-hole log transforms, and the NMR attributes.

CONCLUSION

The prediction of flow zone indicator (FZI) of rocks is essential for the crisp identification of rock types. Delineation of rock types is an essential key element for adequate reservoir characterization. Relationships between the FZI and conventional log measurements and NMR log attributes have been difficult to establish for carbonate rocks, in the past. This is partially due to the haphazard procedure applied in selecting the log measurements for modeling the FZI. This is also largely due to the high level of heterogeneity associated with carbonate rocks. This study provides insights on variables and transforms that impact the rock flow zone indicator.

Dimensional analysis and non-linear regression have been applied to derive transforms that appear to reflect the carbonate rock texture. When these transforms were integrated with NMR log attributes, a significant amount of the flow zone indicator variance appears to have been captured. A general regression neural network has proven to be capable of giving reasonably precise predictions of the rock FZI when the rock texture transforms and NMR log attributes are used as input. The GRNN model consists of building a conditional joint distribution from the training data set. Estimates of the output are performed by calculating the expected value of the conditional target variable, for a known set of input variables. The target estimates converge to actual values only when sufficient input variables that control the behavior of the target variable are used. The introduced relationship between the FZI and NMR attributes and conventional log measurements may be considered a significant leap toward the accurate prediction of FZI for highly complex and heterogeneous carbonate reservoirs.

APPENDIX A

Description of Carbonate Reservoir Data From the M Field

Summary statistics of the M field data are given in Table 2. The data belong to a Lower Cretaceous carbonate reservoir within an elongated onshore domal trap. Open-hole log data consist of SP, GR, SP, resistivity logs, porosity from neutron log, ρ_b, Δt, and P_e. NMR log data consist of FFI, BVI, and T_{2lm}. Core data consist of helium porosity and air permeability for 140 cored depths.

Lithology of the preserved Lower Cretaceous strata consists mainly of clean limestone, and occasional bands of slightly argillaceous limestone rock with up to 5% neomorphic dolomite, and 5-30% of clay minerals. The clay minerals consist of kaolinite, illite, and chlorite in order of abundance. The deposition of this formation appears to have taken place on a shallow low angle platform with minor sea level fluctuations during transgressive regressive cycles. Typically, the oolite reservoir has a segregated fluid distribution vertically. The oil column (gravity = 40^o API) has a thickness of 400 ft, and is supported by an active aquifer zone. Peloidal and skeletal grainstone and packstone dominate with approximately 3-30 % porosity and 0.052 mD to 2150 mD permeability. X-Ray Diffractometric studies on 34 Lower Cretaceous samples show the presence of the following lithofacies:

Rock type 1: Calcareous mudstone: Consists of about 26% shale, 47.3% quartz, 21.1% dolomite, 2% calcite, a small amount of pyrite (1.4%), and a minor potassium-feldspar content of 2.2%. Pyrite exists as pore-filling and appears to have been produced diagenetically during biodegradation of organic matters. The small amount of calcite occurs mostly as carbonate cement.

Rock type 2: Marl: Consisting of carbonate minerals ranging from 42% to 59% with calcite being the dominant mineral. Shale content varies from 15 to 30%. Quartz content varies from 4 to 25%. The highest dolomite content is 3%. Whereas, siderite content gets as high as 17%.

Rock type 3: Argillaceous limestone: Consisting of limestones mixed with approximately 22% shale content dominated by the presence of moderately crystallized kaolinite. Dolomite constitutes about 5% of the composition, whereas pyrite constitutes about 7%.

Rock type 4: Slightly argillaceous dolostone: Consisting of approximately 70% dolomite along with 15% of calcite in its bulk volume. Shale content is as high as approximately 11% with about 4% pyrite content.

Rock type 5: Slightly argillaceous limestone: Consisting of 90% or more limestone with shale content less than 10%, with pyrite concentration ranging from 1.1 to 3.3%.

Rock Type 6: Limestone: Consisting of dominant calcite component ($CaCO_3$) ranging from 91% to 100%. Dolomite fills the rest of the lithology makeup. This rock type is marked by coarse grains which are loosely spaced, connected by isopachous bladed cement.

REFERENCES

Abbaszadeh, M., Fuji, H., and Fujimoto, F. (1996) "Permeability prediction by hydraulic flow units – theory and applications", *SPE Formation Evaluation*, Vol. 11, No. 4, pp. 263-271.

Abedini, A., Torabi, F., and Tontiwachwuthikul, P. (2011) "Rock type determination of a carbonate reservoir using various approaches: a case study", *Special Topics & Reviews in Porous Media-An International Journal*, Vol. 2, No. 4, pp. 293-300.

Aldousari, M., Alomair, O., and Garrouch A.A. (2016) "Investigating the dependence of shear wave velocity on petrophysical parameters", *Journal of Petroleum Science and Engineering*, Vol. 146, pp. 286-296.

Amaefule, J.O., Altunbay, M., Tiab, D., Kersey, D.G. and Keelan, D.K. (1993) "Enhanced reservoir description: using core and log data to identify hydraulic (flow) units and predict permeability in uncored intervals/wells", Paper SPE 26435 presented at the 68th Annual Technical Conference and Exhibition, Houston, TX, USA.

Coates, G.R., Xiao, L., and Prammer, M.G. (1999) NMR Logging Principles and applications, Halliburton Energy Services, Houston.

Corbett, P.W.M. and Mousa, N.I.A. (2010) "Petrotype-based sampling applied in a saturation exponent screening study, Nubian Sandstone Formation, Sirt Basin, Libya", *Petrophysics*, Vol. 51, No. 4, pp. 264-270.

Garrouch, A.A. (1999) "A modified Leverett J-function for the Dune and Yates carbonate fields: A case study", *Energy and Fuel*, Vol. 13, No. 5, pp. 1021-1029.

Garrouch, A.A., and Al-Sultan, A.A. (2019) "Exploring the link between the flow zone indicator and key open-hole log measurements an application of dimensional analysis", *Petroleum Geoscience*, Vol. 25, pp. 1-16.

Ghadami, N., Rasaei, M.R., Hejri, S., Sajedian, A., and Afsari, K. (2015) "Consistent porosity-permeability modeling, reservoir rock typing and hydraulic flow unitization in a giant carbonate reservoir", *Journal of Petroleum Science and Engineering*, Vol. 131, pp. 58-69.

Gunter, G.W., Finneran, J.M., Hartmann, D.J., and Miller, J.D. (1997) "Early determination of reservoir flow units using an integrated petrophysical flow methods", Paper SPE 38679 presented at the Annual Technical Conference and Exhibition, San Antonio, Texas, USA.

Guo, G., Diaz, M.A., Paz, F., Smalley, J., and Waninger, E.A. (2007) "Rock typing as an effective tool for permeability and water-saturation modeling: a case study in a clastic reservoir in the Oriente basin", *SPE Reservoir Evaluation and Engineering*, Vol. 10, No. 6, pp. 730-739.

Lucia, F.J. (2007) Carbonate Reservoir Characterization an Integrated Approach", Springer, 2nd Edition, Berlin.

Michel, R., and Bruno, L. (2014) "Rock typing in carbonates: A critical review of clustering methods", Paper SPE 171759-MS presented at the Abu Dhabi International Petroleum Exhibition and Conference, Abu Dhabi, UAE.

Mirzaei-Paiaman, A., Ostadhassan, M., Rezaee, R., and Jooybari, H.S. (2018) "A new approach in petrophysical rock typing", *Journal of Petroleum Science and Engineering*, Vol. 166, pp. 445-464.

Panjamani, A., DR, M., Moustafa, S., and Al-Arifi, N.S.N. (2016) "Selection of shear modulus correlation for SPT N values based on site response studies", *Journal of Engineering Research*, Vol. 4, No. 3, pp. 167-191.

Prasad, M. (2003) "Velocity-permeability relations within hydraulic units", *Geophysics*, Vol. 68, No. 1, pp. 108-117.

Riazi, Z. (2018) "Application of integrated rock typing and flow units identification methods for an Iranian carbonate reservoir", *Journal of Petroleum Science and Engineering*, Vol. 160, pp. 483-497.

Sneider, R.M., and Erickson, J.W. (1997) "Rock types, depositional history, and diagenetic effects, Ivishak reservoir, Prudoe Bay field", *SPE Reservoir Engineering*, Vol. 12, No. 1, pp. 23-30.

Soleymanzadeh, A., Jamialahmadi, M., Helalizadeh, A., and Soulgani, B.S. (2018) "A new technique for electrical rock typing and estimation of cementation factor in carbonate rocks", *Journal of Petroleum Science and Engineering*, Vol. 166, pp. 381-388.

Specht, D.(1991) "A general regression neural network", *IEEE Trans. On Neural Networks*, Vol. 2, pp. 568-576.